Microelectrochemical Patterning of Surfaces with Polymer Brushes

Cyrine Slim,[†] Yvette Tran,[‡] Mohamed M. Chehimi,[§] Nicolas Garraud,[||] Jean-Paul Roger,[||] Catherine Combellas,[†] and Frédéric Kanoufi*,[†]

Laboratoire Environnement et Chimie Analytique, ESPCI, CNRS UMR 7121, 10 rue Vauquelin, 75231 Paris Cedex 05, France, Laboratoire Physico-Chimie des Polymères et Milieux Dispersés, ESPCI, UPMC Université Paris 6, CNRS UMR 7615, 10 rue Vauquelin, 75231 Paris Cedex 05, France, ITODYS Denis Diderot Université Paris 7, CNRS UMR 7086, 1, rue Guy de la Brosse, 75005 Paris, France, and Laboratoire Photons Et Matière, ESPCI, CNRS UPR A0005, 10 rue Vauquelin, 75231 Paris Cedex 05, France

Received July 25, 2008. Revised Manuscript Received September 3, 2008

Electrogeneration of reducers at a microelectrode allows us to locally debrominate a surface bound polymerization initiator. Once submitted to atom transfer radical polymerization, patterns of nanometer polymer structures are formed on the surfaces. The surface reduction rate, controlled by the microelectrode scan rate and the reducer strength, affects the dimensions of the patterns. The reducer strength allows to tune the surface density of the initiator layer and then the elongation of the polymer brushes grown in the locally etched regions.

Introduction

The design of micropatterned polymer structure is an important issue to develop smart surfaces, actuators, polymer electronics, or biological microsystems. In this respect, different lithographic techniques,[1] including electron-beam lithography,[2] photolithography,[3] microcontact printing,[4] nanoimprinting,[5] Langmuir−Blodgett,[6] or dip-pen[7] lithographies have been used for the micro- and nanofabrication of patterned polymer brushes. Such polymer structures with controlled compositions and dimensions are commonly grown from a wide range of surfaces by atom transfer radical polymerization (ATRP).[8,9] Different bromo-terminated molecules ranging from silanes,[9] thiols[11] or disulfides to aromatic moieties derived from diazonium ions[10] have been proposed to initiate the polymer growth. The density of the polymer brush and therefore its morphology (thickness and folding) are controlled by the density of the polymerization initiator grafted on the surface. This is achieved by diluting the anchored polymerization initiator either by mixing with unreactive molecules,[11] or by partial photochemical[3g,12] or electrochemical[13] decomposition of the initiator seed layer.

Here, we propose to combine two strategies: electrochemistry for the patterning of surfaces with organic moieties and ATRP polymerization to control the growth of polymer nanostructures. The combination of both techniques is an innovative lithography to design smart surfaces. The local control of the density of the surface-bound initiator will be controlled by an electrochemical local probe technique. It should allow the patterning of surface with polymer structure

* Corresponding-Author, E-mail: frederic.kanoufi@espci.fr.
[†] Laboratoire Environnement et Chimie Analytique, ESPCI.
[‡] Laboratoire Physico-Chimie des Polymères et Milieux Dispersés, ESPCI.
[§] ITODYS Denis Diderot Université Paris 7.
[||] Laboratoire Photons Et Matière, ESPCI.

(1) Senaratne, W.; Andruzzi, L.; Ober, C. K. *Biomacromolecules* **2005**, *6*, 2427.
(2) (a) Schmelmer, U.; Jordan, R.; Geyer, W.; Eck, W.; Golzhaüser, A.; Grunze, M.; Ulman, A. *Angew. Chem., Int. Ed.* **2003**, *42*, 559. (b) Ahn, S. J.; Kaholek, M.; Lee, W.-K.; LaMattina, B.; LaBean, T. H.; Zauscher, S. *Adv. Mater.* **2004**, *16*, 2141. (c) He, Q.; Küller, A.; Grunze, M.; Li, J. *Langmuir* **2007**, *23*, 3981.
(3) (a) Husemann, M.; Morrison, M.; Benoit, D.; Frommer, J.; Mate, C. M.; Hinsberg, W. D.; Hedrick, J. L.; Hawker, C. J. *J. Am. Chem. Soc.* **2000**, *122*, 1844. (b) Iwata, P.; Suk-In, P.; Hoven, V. P.; Takahara, A.; Akiyoshi, K.; Iwasaki, Y. *Biomacromolecules* **2004**, *5*, 2308. (c) Zhou, F.; Jiang, L.; Liu, W.; Xue, Q. *Macromol. Rapid Commun.* **2004**, *25*, 1979. (d) Andruzzi, L.; Senaratne, W.; Hexemer, A.; Sheets, E. D.; Ilic, S. B.; Kramer, J. K.; Baird, B.; Ober, C. K. *Langmuir* **2005**, *21*, 2495. (e) Xu, F. J.; Song, Y.; Cheng, Z. P.; Zhu, X. L.; Zhu, C. X.; Kang, E. T.; Neoh, K. G. *Macromolecules* **2005**, *38*, 6254. (f) Konradi, R.; Ruhe, J. *Langmuir* **2006**, *22*, 8571. (g) Khire, V. S.; Harant, A. W.; Watkins, A. W.; Anseth, K. S.; Bowman, C. N. *Macromolecules* **2006**, *39*, 5081. (h) Dong, R.; Krishnan, S.; Baird, B. A.; Lindau, M.; Ober, C. K. *Biomacromolecules* **2007**, *8*, 3082.
(4) (a) Husemann, M.; Mecerreyes, D.; Hawker, C. J.; Hedrick, J. L.; Shah, R.; Abbott, N. L. *Angew. Chem., Int. Ed.* **1999**, *38*, 647. (b) Jones, D. M.; Smith, J. R.; Huck, W. T. S.; Alexander, C. *Adv. Mater.* **2002**, *14*, 1130. (c) vonWerne, T. A.; Germack, D. S.; Hagberg, E. C.; Sheares, V. V.; Hawker, C. J.; Carter, K. R. *J. Am. Chem. Soc.* **2003**, *125*, 3831. (d) Edmondson, S.; Huck, W. T. S. *Adv. Mater.* **2004**, *16*, 1327. (e) Tu, H.; Heitzman, C. E.; Braun, P. V. *Langmuir* **2004**, *20*, 8313. (f) Ma, H.; Li, D.; Sheng, X.; Zhao, B.; Chilkoti, A. *Langmuir* **2006**, *22*, 3751. (g) Azzaroni, O.; Brown, A. A.; Cheng, N.; Wei, A.; Jonasc, A. M.; Huck, W. T. S. *J. Mater. Chem.* **2007**, *17*, 3433. (h) Edmondson, S.; Vo, C.-D.; Armes, S. P.; Unali, G. F. *Macromolecules* **2007**, *40*, 5271. (i) Choi, H.-G.; Amara, J. P.; Swager, T. M.; Jensen, K. F. *Langmuir* **2007**, *23*, 2483.
(5) (a) Beinhoff, M.; Appapillai, A. T.; Underwood, L. D.; Frommer, J. E.; Carter, K. R. *Langmuir* **2006**, *22*, 2411. (b) Genua, A.; Alduncín, J. A.; Pomposo, J. A.; Grande, H.; Kehagias, N.; Reboud, V.; Sotomayor, C.; Mondragon, I.; Mecerreyes, D. *Nanotechnology* **2007**, *18*, 215301.
(6) Brinks, M. K.; Hirtz, M.; Chi, L.; Fuchs, H.; Studer, A. *Angew. Chem., Int. Ed.* **2007**, *46*, 5231.
(7) Hou, S.; Li, Q.; Liu, Z. *Appl. Surf. Sci.* **2004**, *222*, 338.
(8) (a) Matyjaszewski, K.; Xia, J. *Chem. Rev.* **2001**, *101*, 2921. (b) Kamigaito, M.; Ando, T. *Chem. Rev.* **2001**, *101*, 3689. (c) Edmonson, S.; Osborne, V. L.; Huck, W. T. S. *Chem. Soc. Rev.* **2004**, *33*, 14. (d) Brittain, W. J.; Bowes, S. G.; Granville, A. M.; Baum, M.; Mirous, B. K.; Akgun, B.; Zhao, B.; Bickle, C.; Foster, M. D. *Adv. Polym. Sci.* **2006**, *198*, 125. (e) Braunecker, W.; Matyjaszewski, K. *Prog. Polym. Sci.* **2007**, *32*, 93.
(9) (a) Husseman, M.; Malmström, E. E.; McNamara, M.; Mate, M.; Mecerreyes, D.; Benoit, D. G.; Hedrick, J. L.; Mansky, P.; Huang, E.; Russell, T. P.; Hawker, C. J. *Macromolecules* **1999**, *32*, 1424. (b) Matyjaszewski, K.; Miller, P. J.; Suhkla, N.; Immaraporn, B.; Gelman, A.; Luokala, B. B.; Siclovan, T. M.; Kickelbick, G.; Vallant, T.; Hoffmann, H.; Pakula, T. *Macromolecules* **1999**, *32*, 8716.

10.1021/cm8020325 CCC: $40.75
Published on Web 10/10/2008

of controlled morphologies and should provide an interesting alternative to photolithography.[3g]

The scanning electrochemical microscope (SECM) is indeed an ideal tool for the selective chemical micropatterning of surfaces.[14] Generally, a microelectrode is used as a local source of various reactive intermediates able to etch the surface. Our group has shown that highly reducing species electrogenerated at the SECM allowed to etch surfaces as inert as those of fluoro-polymers[15,16] or fluorosilanized[15f] substrates. Further functionnalization leads to functional microdomains surrounded by a highly inert material.[16] Compared to other lithography techniques, the slow writing speed of the SECM is a limitation that may be circumvented either by using a "stamp" electrode[17] or by engaging the fast etching of self-assembled monolayers.[18]

Here, we wish to micropattern surfaces with polymer brushes of controlled density and thickness. Our strategy consists of tuning the density of the surface-bound initiator by a locally controlled electrochemical means. We have focused on the ATRP of 2-(dimethylamino) ethylmethacrylate (DMAEMA) from silicon or glass surfaces grafted with an initiator layer of a bromoisobutyrate alkylsilane (**1**).[19,20] The interest of PDMAEMA lies, on the one hand, in its responsive properties to pH, and on the other hand, in its potentiality in biological applications[1] due to, for example, its bactericide activity. The general procedure used for the selective surface-confined ATRP by SECM is illustrated in Scheme 1. A 25 μm radius microelectrode is held in close vicinity (at 15 μm) of the bromo-terminated initiator grafted surface. It locally generates a reducer, the radical anion, $\mathbf{M}^{\bullet-}$, of an organic redox mediator, **M**.

Scheme 1. Schematic View of the SECM Etching of Surface for Local ATRP Control of PDMAEMA Brushes

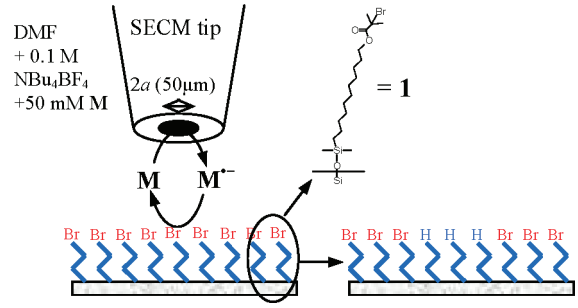

Scheme 2. Schematic View of the Local ATRP Control of PDMAEMA Brushes

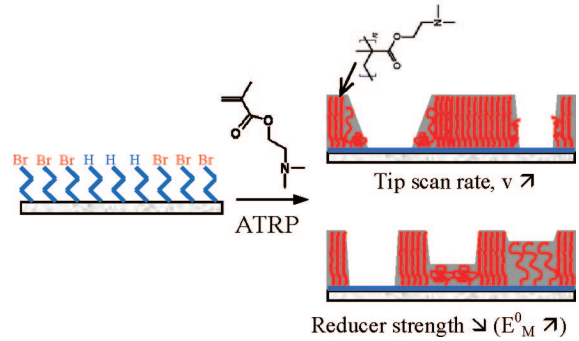

In this work, we will explore the ability of such an electrogenerated reducer to locally decompose the surface bound ATRP initiator (**1**). The electro-assisted decomposition of (**1**) is described from the observation of breath figures, local ellipsometric and XPS measurements of the patterns obtained onto Si or glass surfaces after submission of the locally etched surfaces to ATRP (Scheme 2). We will more particularly describe some parameters that affect the surface decomposition of (**1**) and therefore the polymer patterns dimensions such as the reduction time, the writing speed, and the reducer reductive strength.

Experimental Section

Materials. Standard silicon wafers of 2 in. diameter were purchased from ACS and were cut for use (~ 1 × 1 cm^2). The glass substrates used were microscope slides of 1,1 mm thickness. Glass and silicon substrates were cleaned by treatment with freshly prepared piranha solution (70:30 v/v, concentrated H_2SO_4/aqueous H_2O_2) at 150 °C for 30 min. The substrates were then rinsed with pure water (Millipore, resistivity > 18.2 MΩ.cm), cleaned by ultrasonication in water for 1 min, and dried under nitrogen.

Initiator Monolayer Self-Assembly. Silicon and glass surfaces were covalently grafted by a bromoisobutyrate alkylchlorosilane (11-(2-bromo-2-methyl)propionyloxy)undecyldimethyl-chlorosilane) according to a self-assembling technique described in the literature.[9,20] Briefly, the silane was obtained by (i) esterification

(10) (a) Matrab, T.; Chehimi, M. M.; Perruchot, C.; Adenier, A.; Guillez, V.; Save, M.; Charleux, B.; Cabet-Deliry, E.; Pinson, J. *Langmuir* **2005**, *21*, 4686. (b) Matrab, T.; Chehimi, M. M.; Pinson, J.; Basinska, T.; Slomkowski, S. *Surf. Interface Anal.* **2006**, *38*, 565. (c) Matrab, T.; Chancolon, J.; Mayne L'Hermite, M.; Rouzaud, J.-N.; Deniau, G.; Boudou, J.-P.; Chehimi, M. M.; Delamar, M. *Colloids Surf. A* **2006**, *287*, 217. (d) Matrab, T.; Chehimi, M. M.; Boudou, J.-P.; Benedic, F.; Wang, J.; Naguib, N. N.; Carlisle, J. A. *Diamond Relat. Mater.* **2006**, *15*, 639. (e) Matrab, T.; Save, M.; Charleux, B.; Pinson, J.; Cabet-Deliry, E.; Adenier, A.; Chehimi, M. M.; Delamar, M. *Surf. Sci.* **2007**, *601*, 2357.
(11) (a) Wu, T.; Efimenko, K.; Genzer, J. *J. Am. Chem. Soc.* **2002**, *124*, 9394. (b) Jones, D. M.; Brown, A. A.; Huck, W. T. S. *Langmuir* **2002**, *18*, 1265. (c) Wu, T.; Efimenko, K.; Vlcek, P.; Subr, V.; Genzer, J. *Macromolecules* **2003**, *36*, 2448. (d) Harant, A. W.; Khire, V. S.; Thibodaux, M. S.; Bowman, C. N. *Macromolecules* **2006**, *39*, 1461. (e) Khire, V. S.; Lee, T. Y.; Bowman, C. N. *Macromolecules* **2007**, *40*, 5669.
(12) Yamamoto, S.; Ejaz, M.; Tsujii, Y.; Matsumoto, M.; Fukuda, T. *Macromolecules* **2000**, *33*, 5608.
(13) Wang, X.; Tu, H.; Braun, P. V.; Bohn, P. W. *Langmuir* **2006**, *22*, 817.
(14) (a) Mandler, D. In *Scanning Electrochemical Microscopy*; Bard, A. J.; MirkinM. V., Eds.; Marcel Dekker: New York, 2001, pp 593−627. (b) Wittstock, G.; Burchardt, M.; Pust, S. E.; Shen, Y.; Zhao, C. *Angew. Chem., Int. Ed.* **2007**, *46*, 1584.
(15) (a) Amatore, C.; Combellas, C.; Kanoufi, F.; Sella, C.; Thiébault, A.; Thouin, L. *Chem.—Eur. J.* **2000**, *6*, 820. (b) Kanoufi, F.; Combellas, C.; Shanahan, M. E. R. *Langmuir* **2003**, *19*, 6711. (c) Combellas, C.; Ghilane, J.; Kanoufi, F.; Mazouzi, D. *J. Phys. Chem. B* **2004**, *108*, 6391. (d) Combellas, C.; Kanoufi, F.; Mazouzi, D. *J. Phys. Chem. B* **2004**, *108*, 19260. (e) Combellas, C.; Kanoufi, F.; Mazouzi, D. *J. Electroanal. Chem.* **2006**, *589*, 243. (f) Fuchs, A.; Kanoufi, F.; Combellas, C.; Shanahan, M. E. R. *Colloids Surf., A* **2007**, *307*, 7.
(16) (a) Combellas, C.; Kanoufi, F.; Mazouzi, D.; Thiébault, A. *Polymer* **2003**, *44*, 19. (b) Combellas, C.; Kanoufi, F.; Mazouzi, D.; Thiébault, A. *J. Electroanal. Chem.* **2003**, *556*, 43. (c) Combellas, C.; Fuchs, A.; Kanoufi, F.; Mazouzi, D.; Nunige, S. *Polymer* **2004**, *45*, 4669. (d) Combellas, C.; Kanoufi, F.; Nunige, S. *Chem. Mater.* **2007**, *19*, 3830.
(17) (a) Combellas, C.; Fuchs, A.; Kanoufi, F. *Anal. Chem.* **2004**, *76*, 3612. (b) Sheffer, M.; Mandler, D. *J. Electrochem. Soc.* **2008**, *155*, D203.
(18) Nijhuis, C. A.; Sinha, J. K.; Wittstock, G.; Huskens, J.; Ravoo, B. J.; Reinhoudt, D. N. *Langmuir* **2006**, *22*, 9770.
(19) (a) Zhao, B.; Brittain, W. J. *Macromolecules* **2000**, *33*, 8813. (b) Ejaz, M.; Ohno, K.; Tsujii, Y.; Fukuda, T. *Macromolecules* **2000**, *33*, 2870.
(20) Sanjuan, S.; Perrin, P.; Pantoustier, N.; Tran, Y. *Langmuir* **2007**, *23*, 5769.

Table 1. Polymerization of PDMAEMA on Si Surfaces after Local Reduction by Radical Anions of Selected Redox Mediators

redox mediator M	BQ[a]	$PhNO_2$[b]	DiAcPh[c]	Phthal[d]	22'Dipyr[e]
E^0_M (V vs SCE)	−0.22	−1.08	−1.44	−1.60	−2.10
e (nm)	22 ± 1	23 ± 1	18 ± 1	26 ± 1	31 ± 1
Δ*e* (nm)[f]	0	5 ± 0.5	11 ± 1	22 ± 1	30 ± 2
Δ*e*/*e*	0	0.22	0.61	0.85	>0.96
brush density (nm^{-2})	0.46	0.38	0.16	0.071	<0.01

[a] Benzoquinone. [b] Nitrobenzene. [c] 1,4-Diacetylbenzene. [d] Phthalonitrile. [e] 2,2′-Dipyridyl. [f] Estimated from local ellipsometric measurement except for phthalonitrile, which was estimated from XPS.

of 25.0 mmol of 10-undecen-1-ol with 28.3 mmol of 2-bromoisobutyryl bromide and (ii) hydrosilylation with 22.3 mmol of dimethylchlorosilane.

Initiator Local Electrochemical Reduction. Reduction of the surface-grafted bromoalkane was achieved in a solution of DMF containing 0.1 M NBu_4BF_4 used as the electrolyte and 50 mM mediator by applying a reductive potential to a platinum working ultramicroelectrode (diameter, $\Phi = 50\ \mu m$). The counter electrode was a platinum wire and the reference electrode was Ag/AgCl ($\Phi = 250\ \mu m$). Tetrabutylammonium tetrafluoroborate was synthesized from ammonium tetrafluoroborate and tetrabutylammonium chloride and recrystallized in petroleum ether. The mediators used were benzoquinone, nitrobenzene, phthalonitrile, diacetylbenzene and 2,2′-dipyridyl of respective standard reduction potentials given in Table 1.

The tip was moved by micromotors. The system was kept under nitrogen in a polyethylene bag (glovebag, Aldrich) during the experiment. The humidity in the plastic bag was maintained as low as possible, RH < 0.3, with molecular sieves; this was checked by a hair hygrometer.

Electrochemical procedures were performed in a 5 mL bath. The solution was degassed with nitrogen for 10 min before use and maintained under nitrogen during the whole experiment.

In all electrochemical procedures, potentials were imposed and currents measured by a potentiostat/galvanostat (CH720A, CH Instruments). All potentials are given versus Ag/AgCl.

Surface-Initiated Atom Transfer Radical Polymerization. Once reduced, the substrate was rinsed in acetone. The growth of the PDMAEMA brush was generated from the substrate by atom transfer radical polymerization of 63.6 mmol of 2-(dimethylamino)ethylmethacrylate monomers. An additional free initiator, ethyl-2-bromoisobutyrate (1.27 mmol), was added to the polymerization mixture to provide an overall concentration of ester in the polymerization mixture; this allows the control of the chain growth of both the surface-attached and bulk initiators.[19−21] The polymerization was performed under the experimental conditions already described. It was conducted at 60 °C in a THF/DMF/toluene mixture of monomer and of a catalyst system made of the free initiator, A, of CuBr and HMTETA ligand; the amounts of each product, in mmol, are respectively, [DMAEMA]: 63.7/[A]: 1.27/[Cu^+] 0.382/[HMTETA]: 0.763. After polymerization, the substrate was extensively rinsed in THF and water and then dried under nitrogen.

Ellipsometry. The thickness of the brush inside and outside the areas submitted to local reduction was determined by ellipsometry. The measurements were performed using (i) a Sentech SE 400 apparatus on mm^2 domains and (ii) a microscopic imaging ellipsometer for the micrometer patterns. The light source was a helium−neon laser ($\lambda = 632.8$ nm), and the angle of incidence was set to 70° in (i) and 60° in (ii). The microscopic imaging ellipsometry setup was similar to that proposed by Linke et al.[29] but with a He−Ne laser illumination. For an approximately 100 × 100 μm^2 domain, this ellipsometry setup transforms 4 images obtained with 4 compensator settings into 256 × 252 square pixels images for the two ellipsometry parameters Δ and Ψ, respectively, the phase and amplitude variations introduced by the substrate surface reflection. The microscope does not give absolute Δ and Ψ values but correct relative variations.[29] The ellipsometry phase parameter, Δ, is the most sensitive to the size of coatings deposited onto silicon and a variation of −1.1° per nm of coating is expected, according to the experimental setup (incidence angle 60°) if one assumes the material can be modeled by a single polymer layer with chosen refractive index of $n = 1.517$. The patterned surfaces were analyzed with the ellipsometry microscope and the variations in Δ values were transposed into polymer thicknesses using the absolute Δ-values obtained from the conventional ellipsometer on the known nonreduced domain. By scanning the laser illumination over the whole pattern region and acquiring ellipsometry images, one could fully describe the pattern shape and dimensions with a high resolution (micrometer). The sensibility of the acquisition is then improved by averaging the ellipsometry signal in the direction perpendicular to the laser illumination scanning.

For the conventional ellipsometer, a multilayer model for the film was used for the calculation of the thickness of silica, initiator, and grafted polymer layers from experimentally measured ellipsometry angles, Ψ and Δ. The refractive indices used for the calculations were $n = 1.460$ for the native silica layer, $n = 1.508$ for the initiator layer, and $n = 1.517$ for the PDMAEMA brush.

XPS. XPS spectra were recorded using a Thermo VG Scientific ESCALAB 250 system fitted with a microfocused, monochromatic Al Kα X-ray source (1486.68 eV) and a magnetic lens that increases the electron acceptance angle and hence the sensitivity. An X-ray beam of 650 and 120 μm size was used at voltage of 15 kV and a power of 200 and 22 W for the image and for the line scans respectively. The spectra were acquired in the constant analyzer energy mode, with a pass energy of 150, 20, and 9 eV for, respectively, the survey, the narrow regions, and the image. The Avantage software (version 3.51) was used for data processing. Spectral calibration was determined by setting the aliphatic C−C/C−H C1s peak at 285 eV. The N1s parallel image was recorded over an area of 375 × 500 μm^2 in the constant retard ratio. The image is obtained at the maximum N1s peak (energy 100.3 eV) and substracted from the background taken at 97 eV.

FEMLAB Simulation. The steady-state profiles of chosen dimensionless concentrations of a species, generated at a moving microelectrode, and computed at the surface of an insulating substrate were deduced from the resolution of the convection equations by the finite elements method (FEMLAB environment). The concentration profiles are illustrated for tip scan rates of 5, 50 and 500 μm/s in Figure 3a−c, respectively. For the sake of computational simplicity, the microelectrode has a squared insulating sheath, instead of a circular one, but it does not significantly change the results obtained and the resulting discussion. The active part of the microelectrode, the tip, is the disk (25 μm radius) situated at the center of the square microelectrode (250 × 250 μm^2). The simulation was conducted in a box of dimensions 0.8 × 1.2 × 0.1 mm^3. The electrode is immobile and the underlying box wall (substrate) is moved along the y direction at a rate v_0. The velocity profiles are simplified according to the results presented in ref 17. Between the electrode and the substrate (separated by the distance d) the fluid velocity increases linearly with the height, *z*: $v(z) = v_0(1 - z/d)$. Everywhere else, the fluid is moved at the velocity v_0.

(21) (a) Kong, X.; Kawai, T.; Abe, J.; Iyoda, T. *Macromolecules* **2001**, *34*, 1837. (b) Boyes, S. G.; Akgun, B.; Brittain, W. J.; Foster, M. D. *Macromolecules* **2003**, *36*, 9539.

Results and Discussion

PDMAEMA Growth from Si Surfaces by ATRP. In the special case of the grafting of polymer brushes of PDMAEMA by ATRP from Si surfaces, we have studied the influence on the ATRP of the initiator densities and reaction times with the same reactants mixtures proportions. Within the same reactants mixtures proportions but with different reaction times, the polymer chains formed in the bulk solution have a molecular mass, Mn, ranging from 39 400 to 113 200 g/mol with a polydispersity of $I_p \approx 1.4$. Unlike the ATRP polymerization of *tert*-butyl methacrylate and styrene that produces polymer with a polydispersity lower than 1.1, the ATRP growth of DMAEMA is not as easy to control. This is in agreement with the literature and the value we obtained fits the lowest polydispersity value reported for the controlled polymerization of DMAEMA in solution; a lower and minimum value of 1.25 was obtained by using a lower polymerization temperature or more polar solvents.[22] It has also been shown that the grafted polymer chains could be cleaved and recovered. This is difficult to perform under our conditions because (i) the cleavage of the initiator from the surface is not straightforward and (ii) it requires the use of a high surface area of functionnalized materials. The latter argument cannot be applied in the patterned regions. However, it has been shown that the molecular weights of cleaved and bulk chains were equal, and the polydispersity of cleaved chains was lower than that of of bulk chains.[9a] In our case, we then assumed that the size and the polydispersity of grafted and bulk polymer chains were the same.[20]

On the Si substrate, the grown polymer brushes thickness, e obtained from ellipsometry, is linearly dependent on the bulk polymer molar mass, M_n. A polymer grafting density, σ of about 0.46 nm^{-2} ensues from eq 1

$$\sigma[nm^{-2}] = \frac{e[mm]}{M_n}\rho[g\ cm^{-3}]N_A \times 10^{-21} \qquad (1)$$

where ρ is the PDMAEMA density (1.318 g/cm^3), N_A is the Avogadro number, e is expressed in nm and M_n in g/mol. For the Si substrates used in this work, the average polymer grafting density σ is about 0.46 nm^{-2}. For this specific polymer grafting density, depending on the experimental polymerization conditions (polymerization time or temperature), the polymer layer thickness grown from Si surfaces ranges from 20 to 31 nm (Table 1).

We have also independently demonstrated that the thickness of PDMAEMA polymer brushes grafted by ATRP from Si increased proportionally with the initiator surface coverage, as expected for ATRP.[3g,4a,11−13] The density of **1** was decreased by mixing **1** with alkyl chains that are unreactive toward ATRP. As expected, whatever the initiator density, the polymer mass distribution is the same, and for a given polymer molar mass, in agreement with eq 1, the grafted polymer thickness is also linearly dependent on the polymer grafting density for σ ranging from 0.12 to 0.46 nm^{-2}.[20]

Micropatterning of Si or Glass with PDMAEMA. To pattern Si or glass surfaces with ATRP grown polymers, we can locally prevent the ATRP polymerization process by removal of the polymerization initiating properties of the surface. Such deactivation requires the debromination of the bromo-terminated layer of **1** self-assembled on Si or glass. Such debromination could be obtained from electron transfer reactions. Indeed, the ATRP polymerization relies on the debromination of a polymerization initiator and the polymer growth may be tuned by the precise control of the electron transfer reaction between the metallic catalytic redox center and the polymerization initiator.[8,23] In organic solvents, the reductive debromination of bromoalkanes has been extensively investigated either by homogeneous means (via an electrogenerated electron donor) or heterogeneous means (via an electrode).[24−26] After an exchange of two electrons and one proton, the global reduction (2 + 3) yields the corresponding alkane. The injection of the first electron into the bromoalkane molecule (eq 2) is concerted with the C−Br bond breaking and yields the alkyl radical and a bromide ion according to:

$$RBr + M^{\bullet -}(or + e^-) \rightarrow R^{\bullet} + Br^- + M \qquad (2)$$

Generally, the alkyl radical is more easily reduced than the starting bromoalkane and the alkyl anion formed upon this second electron transfer (eq 3) readily protonates in the medium.

$$R^{\bullet} + M^{\bullet -}(or + e^-) \rightarrow R^- + M \xrightarrow{H^+} RH \qquad (3)$$

When an aromatic electron donor, $M^{\bullet -}$, is used to mediate homogeneously the RBr reduction, the addition product of the alkyl radical issuing from the first electron transfer (eq 2) with the aromatic mediator is also observed.[25] The knowledge of the homogeneous reduction kinetics and thermodynamics of bromoalkanes allows to predict that a surface anchored bromoalkyl chain might be reduced and therefore debrominated by reducing radical anions such as that of 2,2′-dipyridyl ($E^0 = -2.10$ V vs SCE).

This radical anion, named $M^{\bullet -}$, was generated at a microelectrode, of radius $a = 25\ \mu m$, held in the close vicinity of the substrate surface, typically the tip-substrate separation distance, d, was chosen as $d = 0.6\ a$. Because of the small separation distance between the tip and the substrate, the electrogenerated reducer $M^{\bullet -}$ may reduce locally the substrate surface and debrominate it locally. Once

(22) Zhang, X.; Xia, J.; Matyjaszewski, K. *Macromolecules* **1998**, *31*, 5167.

(23) Qiu, J.; Matyjaszewski, K.; Thouin, L.; Amatore, C. *Macromol. Chem. Phys.* **2000**, *201*, 1625.

(24) (a) Andrieux, C. P.; Gallardo, I.; Savéant, J.-M.; Su, K. B. *J. Am. Chem. Soc.* **1986**, *108*, 638. (b) Andrieux, C. P.; Savéant, J.-M.; Su, K. B. *J. Phys. Chem.* **1986**, *90*, 3815. (c) Nadjo, L.; Savéant, J. M.; Su, K. B. *J. Electroanal. Chem.* **1985**, *196*, 23. (d) Lexa, D.; Saveant, J. M.; Su, K. B.; Wang, D. L. *J. Am. Chem. Soc.* **1988**, *110*, 7617.

(25) (a) Daasbjerg, K.; Pedersen, S. U.; Lund, H. *Acta Chem. Scand.* **1989**, *43*, 876. (b) Pedersen, S. U.; Lund, H. *Acta Chem. Scand.* **1991**, *45*, 397. (c) Mikkelsen, K. V.; Pedersen, S. U.; Lund, H.; Swanstrom, P. *J. Phys. Chem.* **1991**, *95*, 8892. (d) Pedersen, S. U.; Lund, T.; Daasbjerg, K.; Pop, M.; Fussing, I.; Lund, H. *Acta Chem. Scand.* **1998**, *52*, 657. (e) Kjærsbo, T.; Daasbjerg, K.; Pedersen, S. U. *Electrochim. Acta* **2003**, *48*, 1807.

(26) (a) Savéant, J.-M. *J. Am. Chem. Soc.* **1987**, *109*, 6788. (b) Savéant, J.-M. *J. Am. Chem. Soc.* **1992**, *114*, 10595. (c) Savéant, J.-M., In *Advances in Physical Organic Chemistry*; Tidwell, T. T., Ed.; Academic Press Ltd., London, 2000; Vol *35*, pp 117−192. (d) Costentin, C.; Robert, M.; Savéant, J.-M. *Chem. Phys.* **2006**, *324*, 30.

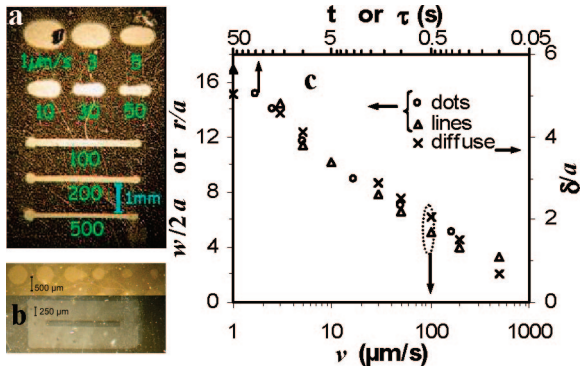

Figure 1. Condensation of water on PDMAEMA brush patterns. Whiter regions are etched. (a.) Si substrate: effect of the tip scan rate on the pattern width. (b) Glass substrate: top, effect of the reduction time on the pattern radius (from left to right 30, 20, 10, 3, 1, 0.3 s); bottom, polymerized band surrounded by reduced zone, writing speed = 200 μm/s. (c) Effect of the microelectrode scan rate, v, or the reduction time, t (or the time-of-flight: $\tau = 2a/v$), on the pattern width, w, or diameter, $2r$, and on the pattern diffuse border length, δ; $w/2$, r, and δ are normalized by the microelectrode radius.

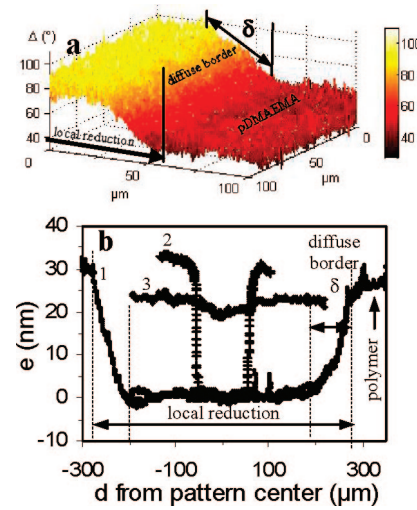

Figure 2. Local ellipsometry of a PDMAEMA brush pattern grown by ATRP on a SECM locally reduced Si surface. (a) Images of the ellipsometric parameter. (b) Evolution of the PDMAEMA thickness, e, along a pattern made by a tip scanned at (1) 5, (2) 500, and (3) 400 μm/s with the (1,2) 2,2'-dipyridyl or (3) nitrobenzene radical anion.

locally reduced, the surface is submitted to polymerization of DMAEMA using ATRP.

Patterns Morphology from Breath Figures. Patterns are observed from surface wettability contrasts evidenced by water condensation figures, also named breath figures.[27] Panel a and b in Figure 1 presents typical condensation figures obtained for a bromo-terminated surface (silicon on the left and glass on the right) locally reduced by the radical anion of 2,2′-dipyridyl and further submitted to the ATRP of DMAEMA. The surface hydrophobicity contrast related to local chemical transformation is detected after local reduction, but it is generally enhanced once the surface has been polymerized. The patterns were obtained either by scanning the surface at different microelectrode scan rates at a constant distance d (Figure 1a), or by holding it at a fixed distance from the substrate for different duration times (Figure 1b). The width of the bands patterned by a moving tip, w, decreases with the tip scan rate (Figure 1a), whereas the radius of the circular patterns etched by a stationary tip, r, increases with the duration of the electrogeneration of the reducer at the tip (Figure 1b). The dimensions of the reduced domains, normalized by the tip radius a ($w/2a$ for the lines, r/a for the dots), are given in Figure 1c as a function of the microelectrode scan rate, v (o), or the reduction time, t (Δ). The concordance of the two abscissa scales is ensured by considering that for the moving tip, the time of reduction at a given position on the substrate is given by the time-of-flight, τ, of this position by the conductive part of the microelectrode.[15e]

$$\tau = 2a/v \qquad (4)$$

There is indeed a good agreement between the dimension of the patterns obtained with a moving or a stationary tip for times longer than 1 s (or scan rates slower than 50 μm/s). At faster scan rates the bands patterns are thinner than the corresponding disks ones as a consequence of the convection induced by the tip movement on the reactant expansion.[28] Transition between the reduced line or dot with the polymer is not harsh but progressive through a diffuse border length, δ, that will be discussed below.

Pattern Morphology from Local Ellipsometry. The extent of polymerization of the substrates was obtained either from global ellipsometry measurements in the area not submitted to local reduction (Table 1), or from homemade imaging ellipsometric microscopy in the patterned regions. Given a local thickness information, the latter microscopic technique allows a fast and quantitative analysis of the extent of the surface polymer grafting. We have used images of the ellipsometric phase parameter Δ, more sensitive to the size of coatings deposited onto silicon to characterize the extent of local surface reduction after polymerization. As already reported,[29] ellipsometric microscopy does not give absolute values of the ellipsometric parameters but correct relative variations. We have used the ellipsometry parameter Δ to characterize the extent of surface reduction after polymerization. The patterned surfaces were analyzed with the ellipsometric microscope and the variations in Δ values were transposed into polymer thicknesses using the absolute Δ-values obtained from the conventional ellipsometer on the nonreduced domain. Figure 2a presents a typical Δ-image of the interface between reduced and non reduced domains of a patterned surface submitted to polymerization. The more reduced the surface, the higher the Δ-value and therefore, the thinner the polymer layer. A complete pattern is reconstructed from superposition of such images, as for example in Figure 2b for patterns obtained in curves 1 and 2 at, respectively, a low and fast microelectrode writing speed. This setup is more convenient than AFM to get images of submillimeter patterned domains such as those we microfabricated.

(27) (a) Beysens, D.; Knobler, C. M. *Phys. Rev. Lett.* **1986**, *57*, 1433. (b) Briscoe, B. J.; Galvin, K. P. *J. Phys. D: Appl. Phys.* **1989**, *23*, 422. (c) López, G. P.; Biebuyck, H. A.; Frisbie, C. D.; Whitesides, G. M. *Science* **1993**, *260*, 647.

(28) Combellas, C.; Fermigier, M.; Fuchs, A.; Kanoufi, F. *Anal. Chem.* **2005**, *77*, 7966.

(29) Linke, F.; Merkel, R. *Rev. Sci. Instrum.* **2005**, *76*, 063701.

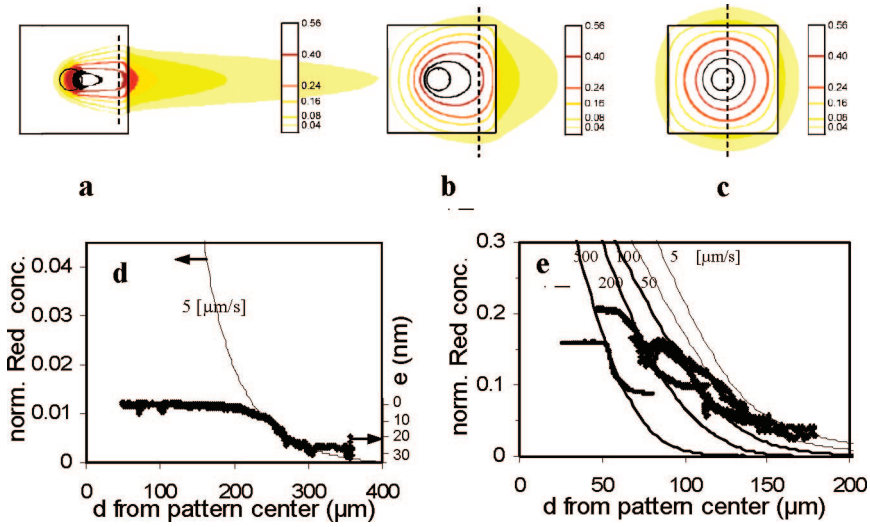

Figure 3. (a−c) Simulated variation of selected normalized concentration profiles of the reducer at the substrate surface. (a) 500, (b) 50, and (c) 5 μm/s. The vertical bar corresponds to the largest lateral expansion of the reducer at the substrate surface. The black central disk corresponds to the metallic part of the microelectrode, radius = 25 μm, the square represents the delimitation of the insulating part of the microelectrode. (d, e) Comparison of the calculated largest lateral expansion of reducer with the experimental ellipsometry profile: (d) 5 μm/s; (e) for fast tip scan rates, from left to right, 500, 200, 100, 50, and 5 μm/s (in e for 5 μm/s the sole concentration profile is presented for comparison with the other rates).

With the radical anion of 2,2′-dipyridyl, no polymer grows in the central reduced region (Figure 2b), mainly because the reduction of **1** is quantitative in this region. It is also observed that between the non reduced domain (higher polymer thickness) and the reduced domain (lower polymer thickness), the polymer thickness decreases gradually and quasi-linearly in a region that defines a "diffuse" boundary. The pattern width estimated from the breath figure corresponds to the whole etched domain ("diffuse" boundaries + central reduced region). The size of the "diffuse" region decreases when the SECM tip is scanned faster (Figure 1c, x symbol), indicating that its physical origin comes from the diffusive-convective transport of the reducer toward the substrate surface.

Convective Origin of the Diffuse Border of the Patterns. Moving a microelectrode over a substrate may generate, at sufficiently large scan rates, a non negligible convective flow in the region of the solution located between the tip and the underlying insulating substrate surface.[28,30] For scan rates faster than 50 μm/s, the convective flow starts to flatten the $\mathbf{M}^{\bullet-}$ concentration profile against the tip but also to drag a trail of $\mathbf{M}^{\bullet-}$ in the microelectrode stream (see simulated concentration profiles in Figure 3a−c). The deformation of the electrogenerated species concentration profile against the microelectrode by this convective flow influences directly the microelectrode current and therefore it affects the process of SECM micropatterning. The influence of this convective flow is experimentally observed on the microelectrode current and fits theoretical simulations (Figure S1). Therefore, such convective contribution must be taken into account to explain the focusing of reactive species at the substrate surface and therefore the shape of the polymer structures patterned at microelectrode writing speeds faster than 50 μm/s.

The steady-state profiles of specific dimensionless concentrations of a species, generated at a moving microelectrode, and computed at the surface of an insulating substrate were deduced from the resolution of the convection equations by the finite elements method (FEMLAB environment). The concentration profiles are illustrated for tip scan rates of 5, 50, and 500 μm/s in Figure 3a−c, respectively. The active part of the microelectrode, the tip, is the disk situated at the center of the square microelectrode. For slow scan rates (see scan rates <50 μm/s in Figure 3a) the concentration profiles are not much affected by the microelectrode movement. For scan rates faster than 50 μm/s (b and c in Figure 3), the convective flow starts to flatten the concentration profile against the tip but also to drag the electrogenerated species trail in the microelectrode stream.

The effect of convection on the surface patterning is illustrated, in the special case of the patterning by the radical anion of 2,2′-dipyridyl, in d and e in Figure 3. As the surface modification involves the chemical transformation of a monolayer, the reduction process involves a very small amount of reducer and the substrate surface behaves as an insulating substrate. Therefore in the "diffuse" region, the extent of the decomposition of **1** is expected to follow the concentration profiles of $\mathbf{M}^{\bullet-}$ at the substrate surface. Indeed, in this region, as observed in Figures 3d,e, the diffuse polymer thinning obtained from ellipsometric microscopy correlates well for different tip scan rates with the largest lateral expansion of the radical anion at the substrate surface obtained from numerical simulations (dashed vertical bar in Figure 3a−c).

To be more specific, for slow scan rates, convection does not affect significantly the concentration profiles; therefore, the patterning resolution is limited by the time-of-flight of the microelectrode over the substrate surface, τ, defined by eq 4. The slower the scan rate, the longer the time-of-flight and the larger the pattern. For example, in Figure 3d at a scan rate of 5 μm/s, the surface reduction of (**1**) starts to be less efficient and the diffuse border begins for a reducer

(30) Nkuku, C. A.; LeSuer, R. J. *J. Phys. Chem. B* **2007**, *111*, 13271.

normalized concentration ≤0.01 (at a distance of 235 μm from the pattern center), whereas with a scan rate of 50 μm/s (Figure 3e), this occurs at a distance of 115 μm from the pattern center and with a 10 times higher normalized concentration of 0.11.

For scan rates faster than 50 μm/s, the convective flow cannot be neglected; the reducer is more concentrated at the center of the tip and is dragged in a longer trail (Figure 3a−c). Correspondingly, the pattern width results from both the influence of the scan rate on the microelectrode time-of-flight and the impact of convection on the concentration profile. Figure 3e shows that the surface begins to get reduced (end of the diffuse border at $d = 150$ μm from the pattern center) for a normalized concentration of about 0.04 at a scan rate of 50 μm/s, whereas with the fastest scan rate (500 μm/s) this situation is observed for a normalized concentration of 0.09 (and a distance of 65 μm from the pattern center), and not 0.3 because at this speed the tip drags a long trail of $\mathbf{M}^{\bullet-}$. This simplified view helps understand the effect of the microelectrode scan rate on the surface patterning resolution. A deeper analysis of the extent of both convection and surface time-of-flight on the surface reduction rate would require the complete description of the surface transformation kinetics, it is out of the scope of this work and is currently under investigation.

The good correlation between the thinning of the polymer in the diffuse region and the reducer concentration profile may also be paralleled to the mechanism of films growth by ATRP, which allows, as was independently demonstrated in the first section, the growth of chains of similar length but with various grafting densities. In the "diffuse" region, the extent of the initiator decomposition, and therefore the final polymer grafting density, is related to the reducer concentration present at the substrate surface. Therefore, it can be inferred that during the SECM patterning of surfaces with polymer brushes, the polymer chains are grown from the whole surface with similar length but in the "diffuse" boundary region, the polymer thinning corresponds to the gradual decrease of the chains grafting density obtained from the gradual decrease of the initiator density. Conveniently, the SECM can then be used to precisely tune, according to the tip scan rate, the grafting of polymer of controlled morphology (thickness) in micrometer domains of controlled dimensions. The local electrochemical etching of the initiator seed layer is then a promising alternative to techniques based on photochemistry.[12] From this study, it is shown that smaller and sharper patterned regions are obtained by limiting the lateral expansion of the reducer. This is obtained at the fastest scan rate, an alternative way would be to drastically decrease the lifetime of the reducer. The latter strategy consists in using a chemical reaction to limit the reactant diffusion and is known as the use of a "chemical lens".[14] Under our experimental conditions, it should be obtained by engaging the reducer $\mathbf{M}^{\bullet-}$ into a competitive reduction with a reducible species (an halogenated aromatic compound for example, or see 16d) present in solution.

Influence of the Reductive Strength of the Electrogenerated Species. A special advantage of the electrochemical nature of the decomposition of the initiator seed layer is that the etching process kinetics can also be tuned by varying the driving force of (2). This can be easily achieved by changing the reducing strength of the tip electrogenerated reducer, simply by changing the aromatic mediator, **M**. Because of the dissociative nature of the first electron transfer to bromoalkanes, the homogeneous reduction of bromoalkanes in solution is known to require a large activation energy,[24,26] indicating that reduction might take place efficiently in a large potential window (>0.4 V). It is then expected that the grafting density of the polymer brush can also be tuned by changing the redox mediator reducing strength, which controls the thermodynamic of the reduction of **1**. We have then performed the local reduction of the bromo-terminated surfaces with different radical anions listed in Table 1. The poorly reducing radical anion of benzoquinone is inactive and does not etch the initiator surface. The local electrochemical generation of any other $\mathbf{M}^{\bullet-}$ yields patterning of the surface. The breath figures show that for the different redox mediators used, except nitrobenzene, the patterns widths are similar for a given tip scan rate (see the Supporting Information, Figure S2). However, the condensation patterns are less contrasted when the reactant used has a lower reducing strength. With the nitrobenzene radical anion, the patterns are similar for slow rates and thinner for rates higher than 10 μm/s or cannot be seen on breath figures beyond 200 μm/s, while they are detected by ellipsometric microscopy (Figure 2b, curve 3).

From local ellipsometry measurements of the etched surfaces (Table 1), the local generation of $\mathbf{M}^{\bullet-}$ results in the growth of polymer patterns of various thicknesses depending on $\mathbf{M}^{\bullet-}$ reductive strength. For weak reducers, the polymer layer grown onto the reduced pattern is thicker and the weaker the reducer, the thicker the polymer layer. With the weakest active reducer, the nitrobenzene radical anion, polymer layers in the reduced patterns are only 6 nm smaller than that on the vicinal substrate surface. Changing the reductive strength then allows to precisely tune the bromine loss of the initiator layer and therefore the surface density (see Table 1) of **1**. This issue is also illustrated by XPS analysis in the spectroscopic or the imaging modes in the case of a surface patterned by the phthalonitrile radical anion (Figure 4). In the imaging mode, the N1s photoelectron region image (Figure 4b) of a straight pattern (ca. 200 μm large) also shows that ATRP confined to the locally etched surfaces yields much lower N surface concentration than the region that has not been reduced. In the spectroscopic mode, Figure 4c shows the lateral variation of XPS spectra taken over a few millimeter line perpendicularly to a large patterned area (typically one made with a tip scanned at 1 μm/s). The N1s signal decreases while the Si2p signal increases when going from the outside to the inside of the pattern (Figure 4d). These results are interpreted owing to the small mean free path of photoelectrons in solids (generally <2−4 nm). If the layer of **1** is not reduced, a thick polymer brush (26 nm) is built that screens the XPS Si2p signal of the silicon substrate. If the bromo-terminated organic layer is reduced, the lower N1s signal indicates that polymerization occurs in the pattern, but results in a thinner and less densely grafted polymer layer (<10 nm). For a homogeneous organic layer

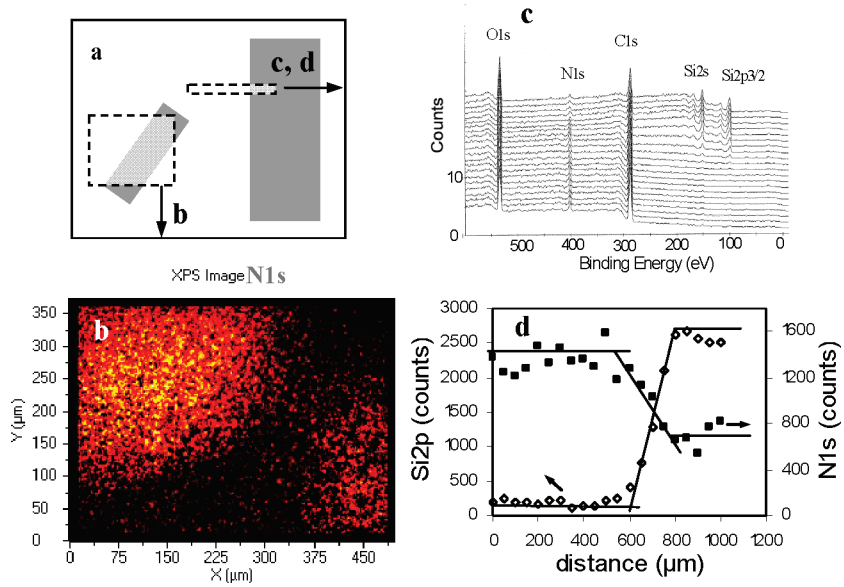

Figure 4. X-ray photoelectron spectroscopy for a Si plate patterned according to Scheme 1. (a) Illustration of the XPS analyses: gray zones are the patterns and the dashed rectangles the domain analyzed by XPS. (b) XPS image of the N1s photoelectron of a 150 μm width oblique pattern. Black parts are locally reduced and deficient in N. (c, d) General spectra or N1s (■) and Si2p peaks (◇) made every 50 μm.

of thickness e containing N atoms covering a substrate (free of N), the XPS N1s signal is expected to fulfill:

$$I_{N1s}(d) = I^{\circ}_{N1s}(1 - \exp(-e/\lambda_{N1s})) \quad (5)$$

where I°_{N1s} is the intensity for a thick film, typically the 26 nm thick polymer film ($I^{\circ}_{N1s} \approx 1300$) and $\lambda_{N1s} \approx 3.3$ nm[10e,31] is the value of the N1s photoelectron inelastic mean free path. In the reduced region, the value of $I_{N1s} \approx 900$ corresponds to photoemission from a 3.7 nm thin film. A "diffuse" border of the pattern is also detected by XPS. The gradual change in the N, Si, and N/Si ratio signals over ca. 200 μm indicates a gradual polymer thinning in this region. Both the dimension of the "diffuse" border found by XPS and the evidence of the presence of the polymer in the reduced zone are consistent with the ellipsometric microscopy measurements.

The decrease in the polymer surface density and therefore of the extent of reduction of the bromo-terminated initiator with the reducer strength (its standard potential, E^0_M) is consistent with processes kinetically governed by electron transfer. At first rough estimate, a Tafel law allows to correlate the activation energy of such process, here the polymer surface density, to the driving force of the rate limiting electron transfer, most likely the first electron transfer from the reducer to the bromo-terminated molecule (2), through a symmetry factor α that describes the reorganization energy required for this rate limiting step

$$[\text{Brush density}] \approx \exp(-\alpha F E^0_M/RT) \quad (6)$$

From the experimental potential dependence of the brush density observed for the 3 intermediates reducers a value of a 0.1 is obtained. It is rather low and agrees with the dissociative nature of the first electron transfer (2) as observed for the reduction of various bromoalkanes in solution ($\alpha \approx 0.3$ for different bromoalkanes).[24,26] Its value is low but comparable to the value observed for the local reductive transformation of chlorinated polymer surface by SECM.[15c]

Conclusion

We have used the SECM in order to etch patterns onto surfaces of polymer brushes of controlled dimension obtained from atom transfer radical polymerization (ATRP). The SECM allows to decompose locally at the micrometer scale a bromo-terminated polymerization initiator seed monolayer, **1**, grafted onto a silicon or a glass substrate. The locally etched surfaces are then submitted to ATRP, which reveals polymer patterns whose morphologies depend on the reduction time and reduction driving force. The initiator decomposition consists in the reductive debromination of the bromo-terminated initiator, **1**, by the radical anion of an organic redox mediator electrogenerated at the microelectrode tip of the SECM. The main results obtained in this work are schematically summarized in Scheme 2. For a given reducer, the faster the tip scan rate, the thinner and less "diffuse" the pattern. For the strongest reducer, the initiator decomposition is quantitative and no polymer grows from the reduced domain. By decreasing the reducer strength, the decomposition rate of the initiator grafted surface is decreased and therefore its surface density. This process was used to grow from Si or glass substrates films of various grafting densities and therefore various thicknesses or elongation in the locally etched regions.

Because the writing process is fast (>500 μm/s), this lithography procedure can be successfully used to design not only empty microdomains surrounded by polymer brushes but also isolated microdomains of polymer brushes (Figure 1b, bottom). With submicrometer microelectrodes[32] combined with the use of ultrashort reduction pulses[33] or

(31) (a) Tanuma, S.; Powell, J. C.; Penn, D. R. *Surf. Interface Anal.* **1994**, *21*, 164. (b) http://www.nist.gov/srd/WebGuide/nist71/71imfp.htm.

"chemical lens",[14] one expects to decrease the patterns dimension and reach a resolution of the order of one μm. We are currently investigating the fabrication and handling of such electrochemical objects. The local electrochemical etching of an initiator seed layer could then present a promising alternative to techniques based on photochemistry. The advantage of this electrochemical method is the ability to control finely the morphology of a given polymer brush pattern, by the adequate choice of the solution electrogenerated reducer. The combination of both techniques is an innovative lithography to design smart surfaces, which should provide an interesting alternative to photolithography.[3g]

(32) Ballesteros Katemann, B.; Schuhmann, W. *Electroanalysis* **2002**, *14*, 22.
(33) Kenney, J. A.; Hwang, G. S. *Nanotechnology* **2005**, *16*, S309.

Acknowledgment. Thibaud Deneulin is acknowledged for his helpful contribution, Tarik Matrab and Carole Bilem are acknowledged for their assistance with XPS measurements. The "Agence Nationale de la Recherche" is acknowledged for its financial support via the ANR-06-BLAN-0368 project.

Supporting Information Available: Additional figures showing the variation of the SECM tip current with the tip scan rate and the variation of the pattern width with the redox mediator reductive strength. This material is available free of charge via the Internet at http://pubs.acs.org.

CM8020325